

Fast analysis system for embossing process simulation of commemorative coin—CoinForm

J. P. Xu¹, Y. Q. Liu^{1,2}, S. Q. Li³ and S. C. Wu⁴

Abstract: For the first time, a special-purpose finite element simulation system CoinForm is developed to analyze the embossing process of commemorative coin, in which one-point reduced integration approach is used in solid element finite element dynamic explicit program. Viscous damping hourglass control algorithm can effectively suppress the spurious modes activated by reduced integration and the computational effort is saved about 93% compared with other method that evaluate anti-hourglass force using stabilization matrix. The embossing process of commemorative coin is then simulated and compared with results from the DEFORM 3D software, which verify the excellent performance of present CoinForm system. According to the flow law of materials from simulation results, this system is found to better improve the geometry of piece for the high quality printed pattern. More importantly, the criterion for positioning the zone of band is obtained in terms of simulation results, which can significantly avoid the defect of light band by optimizing the shape of piece.

Keywords: One-point integration; Hourglass control; Commemorative coin; Embossing process; CoinForm.

1 Introduction

Moulds for embossing of commemorative coin consist of three separate parts: top die, ring die and bottom die. The basic forming process is: the top and bottom dies press the piece when it is put in the ring die. The metal in plastic status is forced

¹ State Key Laboratory of Material Processing and Die & Mould Technology, Huazhong University of Science and Technology, Wuhan, 430074, PR China

² Corresponding author at: State Key Laboratory of Material Processing and Die & Mould Technology, Huazhong University of Science & Technology, 1037 Luoyu Road, Wuhan Hubei 430074, PR China. Tel.: +86 27 87558193; fax: +86 27 87554405; Email: fastamp@vip.sina.com (Liu Yuqi)

³ Shenyang Mint, Shenyang, 110042, PR China

⁴ School of Materials Science and Engineering, Hefei University of Technology, Hefei, 230009, PR China

to flow into the concaves of the top and bottom dies because of the resistance of ring die. With the increasing compression of dies, the surface shape of piece shows the convex pattern. Also the side surface is squeezed to form the required shape since the geometry of the ring die. This process goes on until the depth of pattern satisfies the requirement.

Generally, the international defective rate is 10% all so and even 50% for large diameter coins. With the rapid development of finite element method (FEM) and its wide application (Shaw, Banerjee, and Roy, 2008; Nie, Chang and Fan, 2007), the Computer Aided Engineering (CAE) technology has been drawn more and more attention in the field of bulk forming with distinct advantages (Donoghue, Atluri and Pipkins 1995; Zhao and Hu, 2000; Wang, Liu and Wang, 2000). However, few researches are found to study the embossing process and defect analyses on commemorative coin. Therefore it is necessary to develop specialized software package for embossing process simulation of the commemorative coin.

During the past decade, many practical one-point or multiple-points integration solid-shell and solid elements have been presented (Lee, Cho, Lee, 2002; Basar and Kintzel, 2003; Gato, and Shie, 2008; Cui, Liu, and et al. 2008; Xu, Liu and Du 2008). First, Flanagan and Belytschko (1981) proposed two hourglass control schemes for 2D and 3D problems: viscous and elastic, but they required user-defined parameters to control hourglass force. Belytschko, Ong, Liu and Kennedy (1984) developed an updated hourglass control to eliminate rank deficiency of stiffness matrix, and the constructed hourglass shape vectors met the consistency conditions to pass patch test. Liu, Ong and Uras (1985) then expanded B matrix in a Taylor series about the element centre up to bilinear terms to get six gradient sub-matrices, and the six hourglass forces were obtained according to general three dimension constructive law. Koh and Kikuchi (1987) used DRI (Directional Reduced Integration) method along one or two referential coordinate directions to stabilize mainly 2D element without locking problems. Belytschko and Binderman (1993) developed one-point integration solid element with hourglass control and four-points integration without hourglass control, named ASQBI or ADS element. Only the non-constant part of standard strain field was projected to an assumed strain field, so the volumetric locking of incompressible materials, shear locking and hourglass modes in thin plate were removed successfully. Using B-matrix method in reference (see Liu, Ong and Uras 1985), Liu, Hu and Belytschko (1994) adopted strain gradient sub-matrices related to shear strain terms in co-rotational coordinate system to eliminate shear locking, and then developed NUHEXIN-4 solid element with four-points integration. Based on Liu's method (Liu, Hu and Belytschko, 1994), stress and strain were expanded in a Taylor series about the element centre up to bilinear terms, and the constant part of stress was used to cal-

culate internal force and non-constant part. This could be obtained by simplified constructive matrix and corresponding strain, to calculate hourglass force. Thus, the locking problems were controlled effectively in reference (Hu and Nagy, 1997; Filho and Awruch, 2004). One-point integration solid element with hourglass control, named Jet3D element by Li and Cescotto (1997), could be applied in large deformation nonlinear elastic-plastic problems. In their work, rank sufficiency of stiffness matrix made the element stable, assumed strain method made the element isochoric everywhere to remove volumetric locking, and setting some shear parameters automatically linked with the studied structural dimension effectively avoided shear locking. Liu, Guo and Tang (1998) proposed HEXDS solid element for large deformation nonlinear elastic-plastic problems by adding return mapping algorithm in the previous NUHEXIN-4 solid element for updating stress and strain. Wang and Wagoner (2005) presented WW3D solid element for large deformation nonlinear problems, which was characterized by assumed strain method for avoiding volumetric locking in nearly incompressible or incompressible materials, absent of strain terms corresponding with shear locking and hourglass modes and FI method. Constructing new stability matrix based on Hu-Washizu variation principle, Fredriksson and Ottosen (2007) discussed the value of E_n matrix of regular and irregular element in details.

Based on one-point integration solid element, specialized simulation system named CoinForm for embossing process simulation of commemorative coin is developed in present work, and many simulation cases are executed successfully in this system. Some embossing examples are carried out in the 3rd section, and conclusion has been drawn that this system exhibits higher accuracy and efficient by comparing with the results of Deform 3D. The origin of light band and the criterion for predicting the zone of this band are given out in 4th section, which would assist designers to avoid defect.

2 Viscous damping hourglass control algorithm

2.1 Eight-node solid element model

Solid element in nature coordinate system is shown in Fig. 1, with eight nodes for every element and three translation degrees but no rotation degrees of freedom every node. ξ , η , ζ are three axes of the nature coordinate system. The spatial coordinates x_i in element are approximated in terms of nodal coordinates x_j^i

$$x_i = \sum_{j=1}^8 N_j x_j^i \quad (1)$$

Where, x_i denotes i th spatial coordinate, x_j^i denotes i th spatial coordinate of j th node where i ranges from one to three and j ranges from one to eight, respectively.

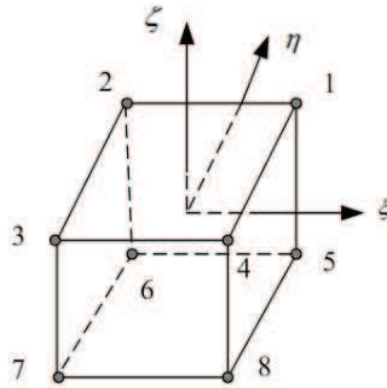


Figure 1: Hexahedral element in nature coordinate system

The trilinear shape function is expressed as

$$N_j = (1 + \xi_j \xi)(1 + \eta_j \eta)(1 + \zeta_j \zeta) / 8 \tag{2}$$

Where (ξ_j, η_j, ζ_j) denotes j th node's nature coordinate, and the values of them are listed in Table 1.

Table 1: Nature coordinate values

	$j=1$	$j=2$	$j=3$	$j=4$	$j=5$	$j=6$	$j=7$	$j=8$
ξ_j	1	-1	-1	1	1	-1	-1	1
η_j	1	1	-1	-1	1	1	-1	-1
ζ_j	1	1	1	1	-1	-1	-1	-1
$\xi_j \eta_j$	1	-1	1	-1	1	-1	1	-1
$\eta_j \zeta_j$	1	1	-1	-1	-1	-1	1	1
$\zeta_j \xi_j$	1	-1	-1	1	-1	1	1	-1
$\xi_j \eta_j \zeta_j$	1	-1	1	-1	-1	1	-1	1

Isoparametric element is applied in this program, so displacement of an arbitrary point in element is interpolated by

$$u_i = \sum_{j=1}^8 N_j u_j^i \tag{3}$$

Where, u_j^i denotes i th displacement degree of freedom of j th node

Elemental shape function matrix notes

$$\mathbf{N}_{3 \times 24} = \begin{bmatrix} N_1 & 0 & 0 & N_2 & 0 & 0 & \cdots & N_8 & 0 & 0 \\ 0 & N_1 & 0 & 0 & N_2 & 0 & \cdots & 0 & N_8 & 0 \\ 0 & 0 & N_1 & 0 & 0 & N_2 & \cdots & 0 & 0 & N_8 \end{bmatrix} \quad (4)$$

Strain gradient operator is expressed as

$$\mathbf{L}_{6 \times 3}^T = \begin{bmatrix} \frac{\partial}{\partial x} & 0 & 0 & \frac{\partial}{\partial y} & 0 & \frac{\partial}{\partial z} \\ 0 & \frac{\partial}{\partial y} & 0 & \frac{\partial}{\partial x} & \frac{\partial}{\partial z} & 0 \\ 0 & 0 & \frac{\partial}{\partial z} & 0 & \frac{\partial}{\partial y} & \frac{\partial}{\partial x} \end{bmatrix} \quad (5)$$

Strain gradient matrix,

$$\mathbf{B}_{6 \times 24} = \mathbf{L}_{6 \times 3} \mathbf{N}_{3 \times 24} \quad (6)$$

Jacobian matrix $\mathbf{J}_{3 \times 3}$ is introduced for calculating strain gradient matrix $\mathbf{B}_{6 \times 24}$,

$$\mathbf{J}_{3 \times 3} = \begin{bmatrix} \frac{\partial x}{\partial \xi} & \frac{\partial x}{\partial \eta} & \frac{\partial x}{\partial \zeta} \\ \frac{\partial y}{\partial \xi} & \frac{\partial y}{\partial \eta} & \frac{\partial y}{\partial \zeta} \\ \frac{\partial z}{\partial \xi} & \frac{\partial z}{\partial \eta} & \frac{\partial z}{\partial \zeta} \end{bmatrix} \quad (7)$$

$$\begin{bmatrix} \frac{\partial N_j}{\partial x} \\ \frac{\partial N_j}{\partial y} \\ \frac{\partial N_j}{\partial z} \end{bmatrix} = \mathbf{J}_{3 \times 3}^{-1} \begin{bmatrix} \frac{\partial N_j}{\partial \xi} \\ \frac{\partial N_j}{\partial \eta} \\ \frac{\partial N_j}{\partial \zeta} \end{bmatrix} \quad (8)$$

thus, $\mathbf{B}_{6 \times 24}$ can be evaluated from Eq. (6).

Strain vectors,

$$\boldsymbol{\epsilon}_{6 \times 1} = \mathbf{B}_{6 \times 24} \mathbf{U}_{24 \times 1} = \mathbf{L}_{6 \times 3} \mathbf{N}_{3 \times 24} \mathbf{U}_{24 \times 1} \quad (9)$$

Where $\mathbf{U}_{24 \times 1}$ denotes nodal displacement vector in element level.

Stress vectors

$$\boldsymbol{\sigma}_{6 \times 1} = (\sigma_{xx}, \sigma_{yy}, \sigma_{zz}, \sigma_{xy}, \sigma_{yz}, \sigma_{zx})^T \quad (10)$$

Which is calculated by

$$\boldsymbol{\sigma}_{6 \times 1} = \mathbf{D}_{6 \times 6} \boldsymbol{\epsilon}_{6 \times 1} \quad (11)$$

Where $\mathbf{D}_{6 \times 6}$ denotes constitutive matrix.

2.2 Volume integration of solid element

Internal force vector in finite element formulation is expressed as the following,

$$\mathbf{F} = \sum \int_V \mathbf{B}^T(\xi, \eta, \zeta) \boldsymbol{\sigma}(\xi, \eta, \zeta) dV \tag{12}$$

where, \mathbf{F} denotes the internal force vector, \mathbf{B} is the strain gradient matrix, $\boldsymbol{\sigma}$ is the stress vector, V is the element domain, and ξ, η, ζ are three axes of the nature coordinate system respectively.

Suppose that

$$\mathbf{g}(\xi, \eta, \zeta) = \mathbf{B}^T(\xi, \eta, \zeta) \boldsymbol{\sigma}(\xi, \eta, \zeta) \tag{13}$$

Using Gauss quadrature method for Eq. (12), then,

$$\int_V \mathbf{g} dV = \int_{-1}^1 \int_{-1}^1 \int_{-1}^1 \mathbf{g} \|\mathbf{J}\| d\xi d\eta d\zeta \tag{14}$$

So it is approximate to that,

$$\int_V \mathbf{g} dV = \sum_{j=1}^n \sum_{k=1}^n \sum_{l=1}^n \mathbf{g}_{jkl} \|\mathbf{J}\| w_j w_k w_l \tag{15}$$

where w_j, w_k, w_l denotes the weight coefficients, generally, they are all set to be 2 for four-points integration; $\|\mathbf{J}\|$ denotes determinant of Jacobian matrix; $\mathbf{g}_{jkl} = \mathbf{g}(\xi_j, \eta_k, \zeta_l)$, n denotes the number of integration points. Especially for one-point integration, $\int_V \mathbf{g} dV = 8 \|\mathbf{J}(0, 0, 0)\| \mathbf{g}(0, 0, 0)$, Element volume can be approximately $Ve = 8 \|\mathbf{J}(0, 0, 0)\|$.

It could save many computations in calculating the strain gradient matrix since the derivatives of shape function are symmetric in element center,

$$\begin{bmatrix} \frac{\partial N_1}{\partial x_i} = -\frac{\partial N_7}{\partial x_i} & \frac{\partial N_2}{\partial x_i} = -\frac{\partial N_8}{\partial x_i} \\ \frac{\partial N_3}{\partial x_i} = -\frac{\partial N_5}{\partial x_i} & \frac{\partial N_4}{\partial x_i} = -\frac{\partial N_6}{\partial x_i} \end{bmatrix} \tag{16}$$

where N_j denotes shape function of j th node and (ξ_j, η_j, ζ_j) nature coordinates of j th node. One-point integration (RI) can save much memory since full integration (FI) must store stress, strain and strain gradient matrix at eight integration points. The strain gradient matrix storage of RI is one-sixteenth of FI, and the stress, strain storage is one-eighth. Suppose that adds, subtracts, multiplies, divides are equal in cost of computation time, calculation of internal force in RI is about one-seventeenth of FI, and update of stress and strain is approximately one-eighth.

2.3 Hourglass control algorithm

Generally, reduced integration methods are used to avoid locking problems in the solution of Eq. (12). Among all the reduced integration methods and other integration methods (Wu, Liu, Zhang and Zhang, 2008 and 2009), one-point method is the most effective and economic which are discussed above. This integration method successfully suppress volume lock and shear lock, however it will suffer hourglass modes. Here, damping hourglass control method (Flanagan and Belytschko, 1981; Hallquist, 2006) is adopted to eliminate the hourglass phenomenon. The excellent simulation results without hourglass modes are given out in next section. The expression of this hourglass control method is in the following, also see (Xu, Liu and Zhang 2008; Xu, Liu and Du 2009).

Viscous hourglass force along x_i axis of every node is defined as,

$$f_{ik}^{hg} = a_h \sum_{j=1}^4 h_{ij} \Gamma_{jk} \quad i = 1, 2, 3 \quad k = 1, 2, \dots, 8 \quad (17)$$

$$a_h = Q_{hg} \rho V_e^{2/3} C / 4 \quad (18)$$

In Eq. (17), f_{ik}^{hg} denotes viscous hourglass force, a_h denotes hourglass coefficient, h_{ij} is the modal of hourglass, and it could be evaluated from the equation $h_{ij} = \sum_{k=1}^8 \dot{u}_i^k \Gamma_{jk}$, where Γ_{jk} denotes hourglass base vectors in Table 2, \dot{u}_i^k the velocity of k th point in i th direction. In Eq. (18), V_e denotes the element volume, C the material sound speed, E the Young's modulus, μ Poisson's ratio, ρ material density, and Q_{hg} a user-defined constant, usually set to a value between 0.05 and 0.15.

Compared with the stabilization hourglass method (Hu and Nagy, 1997; Filho and Awruch, 2004), the calculation cost of anti-hourglass force in this system is cut down to 93%, which verifies the effectiveness of this hourglass method again.

Table 2: Hourglass base vectors

	Γ_{j1}	Γ_{j2}	Γ_{j3}	Γ_{j4}	Γ_{j5}	Γ_{j6}	Γ_{j7}	Γ_{j8}
$j=1$	1	-1	1	-1	1	-1	1	-1
$j=2$	1	1	-1	-1	-1	-1	1	1
$j=3$	1	-1	-1	1	-1	1	1	-1
$j=4$	1	-1	1	-1	-1	1	-1	1

3 Embossing examples for commemorative coin

3.1 Examp^ls analyses with CoinForm system

In embossing simulation, the number of solid element is up to 3 million, so the storage and calculation are much expensive if the FI method or multiple-points integration is adopted, so the advantage of one-point integration is exposed. All the number of meshes in each example is in the limit of one million since the author’s computer’s memory is 2G.

Fig. 2, Fig. 3 and Fig. 4 show the top die, ring die and bottom die respectively in case one , which are provided by Shenyang Mint. The section of coin is shown as Fig. 5. Section for extrusion generates extruded meshes in z direction and section for revolution generates revolved meshes around z direction. It should be noted that the geometry dimension is much small, about 30mm in diameter, and the forming precision requests much high. So four layers mesh in thickness direction is adopted, and the initial mesh number is 44760, node number is 56375. The adaptive mesh refine level is 2. The speed and total displacement of top die is 6m/s and 0.75mm respectively. Aluminum material is adopted, and its hardening curve and parameters are founded in Table 3.

Table 3: Material model and parameters

Material	Young’s modulus (MPa)	Poisson’s ratio	Yield stress (MPa)	hardening curve σ (MPa)	friction coefficient
Al6111	69000	0.33	200	$\sigma = 548.9(\epsilon+0.001)^{0.235}$	0.08



Figure 2: Top die

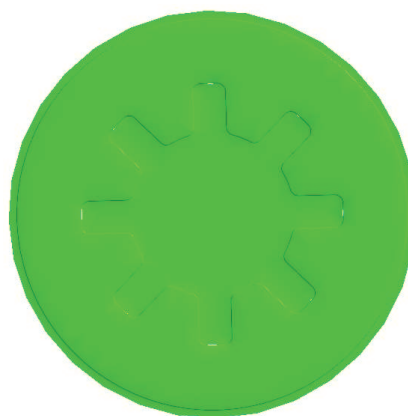


Figure 3: Bottom die

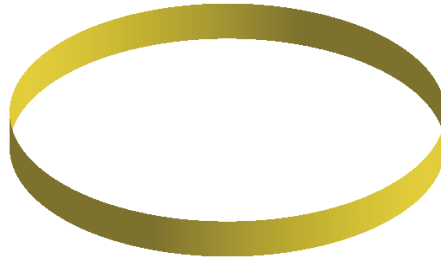


Figure 4: Ring die

Fig. 6 shows the deformed shape of coin, the final mesh number is 311892 and node number is 399620, total CPU time is 1.0 hours. In the region including characters and large deformation, the pattern is described considerably clear. Form the deformed result (mesh picture isn't given out because of the enormous meshes), as shown in Fig. 6, obviously, the hourglass modes are eliminated by damping hourglass control method successfully. Fig. 7 and Fig.8 demonstrate the strain contour and stress contour of the first layer elements respectively.

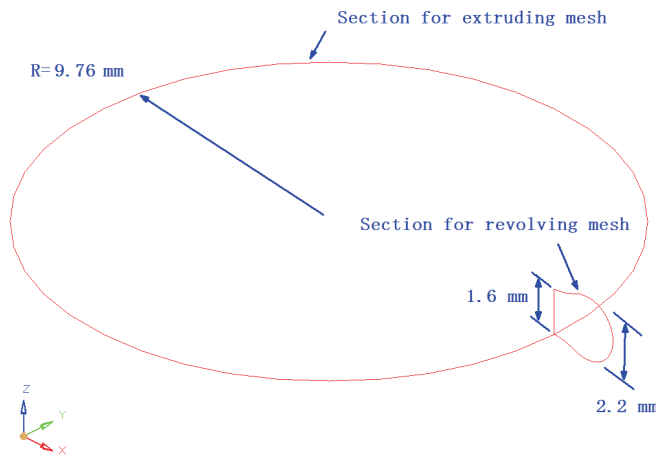


Figure 5: Sections of commemorative coin

3.2 Examples analysis with Deform 3D

The above embossing process is also implemented in DEFORM 3D software. Piece is meshed with tetrahedral element which is a little stiff. The initial number is



Figure 6: Deformed simulation result

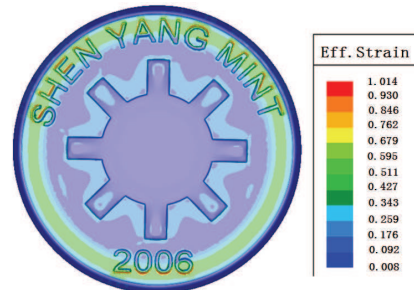


Figure 7: Effective strain contour of the first layer elements

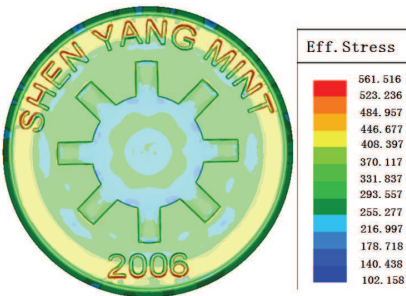


Figure 8: Effective stress contour of the first layer elements



Figure 9: Simulation result of DEFORM 3D

185739. The process parameters settings are all the same as that in CoinForm, total CPU time is 6 hours. The deformed result is as shown in Fig.9.

Considering the result and costs of the same simulation, CoinForm system shows better performance than DEFORM 3D. In one hand, the mesh number is limited to be 200000 in DEFORM 3D, so it can't describe tiny features of the coin clearly. On the other hand, damping hourglass control algorithm used in CoinForm is the most effectively one in all hourglass control algorithms with one-point integration method (Belytschko and Binderman,1993; Hu and Nagy,1997; Filho and Awruch,2004; Li and Cescotto,1997). The author have ever adopted four-points integration method in solving internal force without hourglass control (Belytschko and Binderman,1993; Liu, Hu and Belytschko,1994; Liu,Guo and Tang,1998), but

found that it required large storage and CPU time.

4 Discussion

One main task of this simulation system is to analyze the origin of light band, and to present the solution to avoiding such defect.

4.1 Origin of light band

As shown in Fig. 10, it demonstrates the displacement path of top edge surface of piece in case one. The displacements in radial direction of materials in torus zone one ($r_1 = 11.48, d_1 = 1.2$) are larger than other zones, which will lead to larger slide friction between the top surface and top die. The materials in zone one contact the top die inseparably and come with intensive friction during the whole embossing process. With those friction forces, materials in the zone one flow into zone two ($r_2 = 11.6, d_2 = 1.4$). The light band will be formed in zone two if the friction work in XY plane exceeds one limit value.

A conclusion could be presented by the above analysis that, for a certain material, the light band will come up if the friction work p in a zone exceeds the p_{limit} . One task of our simulations is to find out the limit value. Aluminum, its parameters shown in Table 3, is adopted in the following examples. According to many various tools used in the simulations, a set of maximum work in XY plane is obtained in Table 4.

Define that $p_{\text{limit}} = \alpha p_{\text{ave}} = 0.9 \times 1.04\text{J} = 0.936\text{J}$ with $\alpha = 0.9$.

Table 4: Maximum friction work in various examples

Maximum work (J)	Case 1	Case 2	Case 3	Average
before piece modified	1.01	1.12	0.99	1.04
after piece modified	0.66	0.63	0.65	

4.2 Elimination of light band

The above analysis about the origin of light band provides method to eliminate the light band. Decreasing the radial displacements in zone one by modifying the shape of piece would make the maximum friction work in this zone under the limit work. The modified piece is as shown in Fig. 11, also we get a set of maximum work in radial direction in Table 4. It is found that they are all under the limit, so the band is removed theoretically. Fig.12 demonstrates displacement path of top edge surface of piece modified in case one. We can see that the radial displacement vanishes, so

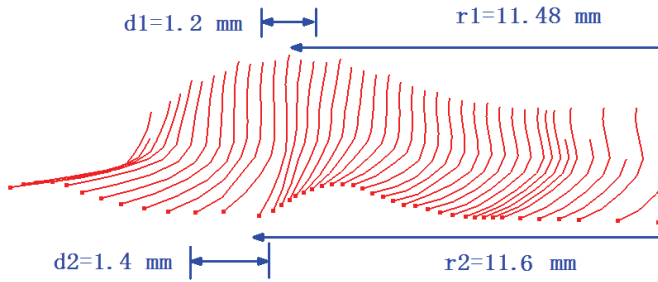


Figure 10: Displacement of top edge surface

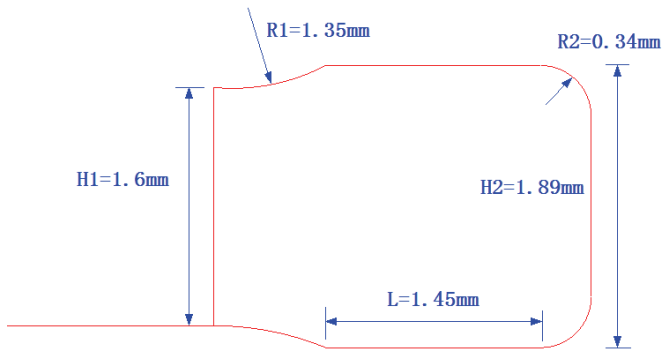


Figure 11: Section of modified piece

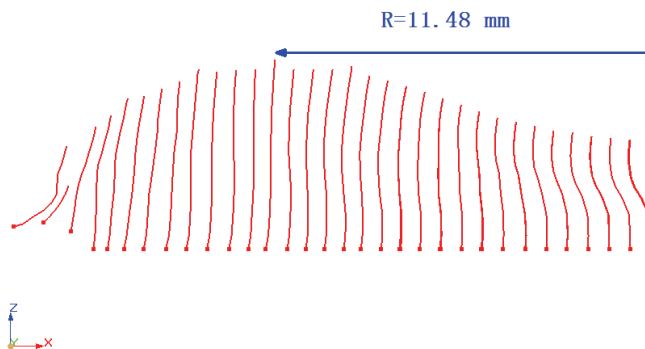


Figure 12: Displacement of top edge surface after piece modified

the corresponding friction work is largely cut down. As to the practical verification of such modified piece, it needs further collaboration with Shenyang Mint.

5 Conclusions and discussions

The first professional CoinForm simulation system for embossing commemorative coin is presented, also its high effectiveness and accuracy are verified by comparing with the results of DEFORM 3D. This system is characterized by the following,

- 1) Aspect of computation: Damping hourglass control is the most economical method of all, meanwhile, the computation of internal force and strain-stress in this system decreases largely comparing with multi-points methods. The fatal disadvantage of one-point integration is occurrence of spurious modes, which would spread to other regions of the model if they appear. With the die speed of 6m/s, damping algorithm suppresses the spurious modes successfully which is demonstrated in the above example.
- 2) Aspect of precision: The accurate contact algorithm, return mapping algorithm and adaptive mesh refine technology make this simulation system could detect plastic fronts in the tiny characteristic region of the coins.

The origin of light band and its distribution criterion are reported in this research. This directs engineers to present practical scheme that changing the edge shape of piece could avoid the occurrence of light band effectively. The modified piece demonstrates less friction work in radial direction which is verified in section 4.

Meanwhile, there are two following advantages for modified piece.

Clearance between piece and ring die decreases, which is beneficial to fill the gaps among ring, top and bottom die, also beneficial to make the printed pattern more perfect.

Squeezed degree of materials in edge inner region of piece decreases, which is beneficial to avoid mesh distortion during simulation.

Acknowledgement: The support of the National Natural Science Foundation of China under project No.: 50575080, National Key Technology R&D Program (No. 2006BAF01A43) and the grant from Shenyang Mint on ‘Simulations of Embossing Processes for Commemorative Coins’ are gratefully acknowledged.

Reference

Basar, Y.; Kintzel, O. (2003): Finite rotations and large strains in finite element shell analysis. *CMES: Computer Modeling in Engineering & Sciences*, 4: 217-230.

- Belytschko, T.; Ong, J.S.J.; Liu, W.K.; Kennedy, J.M.** (1984): Hourglass control in linear and nonlinear problems. *Comp Methods Appl Mech Eng*, 43: 251-276.
- Belytschko, T.; Bindeman, L.P.** (1993): Assumed strain stabilization of the eight-node hexahedral element. *Comp Methods Appl Mech Eng*, 105: 225-260.
- Cui, X.Y.; Liu, G. R.; Li, G. Y.; Zhao, X.; Nguyen, T.T.; Sun, G.Y.** (2008): A Smoothed Finite Element Method (SFEM) for Linear and Geometrically Nonlinear Analysis of Plates and Shells. *CMES: Computer Modeling in Engineering & Sciences*, vol.28, no.2, pp.109-125.
- Donoghue, P.E.O.; Atluri, S.N.; Pipkins, D.S.** (1995): Computational strategies for fatigue crack growth in three dimensions with application to aircraft components. *Engineering Fracture Mechanics*, 52(1):51-64.
- Flanagan, D.P.; Belytschko, T.** (1981): A uniform strain hexahedron and quadrilateral with orthogonal hourglass control. *Int J Num Methods Eng*, 17: 679-706.
- Filho, L.A.D.; Awruch, A.M.** (2004): Geometrically nonlinear static and dynamic analysis of shells and plates using the eight-node hexahedral element with one – point integration. *Finite Element in Analysis and Design*, 40: 1297-1335.
- Fredriksson, M.; Ottosen, N.S.** (2007): Accurate eight-node hexahedral element. *Int J Num Methods Eng*, 72: 631-657.
- Gato, C.; Shie Y.** (2008): Numerical Simulations of Dynamic Fracture in Thin Shell Structures. *CMES: Computer Modeling in Engineering & Sciences*, vol.33, no.3, pp.269-292.
- Hallquist, J.O.** (2006): *LS-DYNA Theory Manual*. 40-42.
- Hu, Y.K.; Nagy, L.I.** (1997): A one-point integration eight-node brick element with hourglass control. *Computer & Structure*, 65: 893-902.
- Koh, B.C.; Kikuchi, N.** (1987): New improved hourglass control for bilinear and trilinear elements in anisotropic linear elasticity. *Comp Methods Appl Mech Eng*, 65: 1-46.
- Lee, K.; Cho, C.; Lee, S.W.** (2002): A geometrically nonlinear nine-node solid shell element formulation with reduced sensitivity to mesh distortion. *CMES: Computer Modeling in Engineering & Sciences*, 3: 339-349.
- Li, K.P.; Cescotto, S.** (1997): An 8-node brick element with mixed formulation for large deformation analysis. *Comp Methods Appl Mech Eng*, 14: 157-204.
- Liu, W.K.; Ong, J.S.J.; Uras, R.A.** (1985): Finite element stabilization matrices-a unification approach. *Comp Methods Appl Mech Eng*, 53: 13-46.
- Liu, W.K.; Hu, Y.K.; Belytschko, T.** (1994): Multiple integration under-integrated finite elements. *Int J Num Methods Eng*, 37: 3263-3289.

Liu, W.K.; Guo, Y.; Tang, S. (1998): A Multiple-integration eight-node hexahedral finite element for large deformation elasto-plastic analysis. *Comp Methods Appl Mech Eng*, 154: 69-132.

Nie, Y.F.; Chang, S.; Fan, X.K. (2007): The Parallel Mechanism of Node-Based Seamless Finite Element Method. *CMES: Computer Modeling in Engineering & Sciences*, vol.19, no.2, pp.135-143.

Shaw, A.; Banerjee, B.; Roy, D. (2008): A NURBS-based Parametric Method Bridging Mesh-free and Finite Element Formulations. *CMES: Computer Modeling in Engineering & Sciences*, vol.26, no.1, pp.31-57.

Wang, J. W.; Liu, Z.; Wang, B. Y. (2000): Study on the finite deformation elasto-plastic FEM for bulk forming. *Journal of plasticity engineering*, 7(1): 41-44.

Wang, J.; Wagoner, R.H. (2005): A practical large-strain solid finite element for sheet forming. *Int J Num Methods Eng*, 63: 473-501.

Wu, S.C.; Liu, G.R.H.; Zhang, O.; Zhang, G.Y. (2008). A node-smoothed point interpolation method (NS-PIM) for three-dimensional thermoelastic problems. *Numerical Heat Transfer, Part A: Applications*, 54(12): 1121-1147.

Wu, S.C.; Liu, G.R.H.; Zhang, O.; Zhang, G.Y. (2009): A node-based smoothed point interpolation method (NS-PIM) for thermoelastic problems with solution bounds. *International Journal of Heat and Mass Transfer*, 52(5-6): 1464-1471.

Xu, J.P.; Liu, Y.Q.; Du, T.; Zhang, Z.B. (2009): Application of solid element in ironing simulation and optimization of process parameters. *China Mechanical Engineering*. In Press.

Xu, J.P.; Liu, Y.Q.; Zhang, Z. B.; Du, T. (2008): Finite element dynamic explicit method in ironing process simulation. *Forging & Stamping Technology*, 33(5): 38-43.

Xu, J.P.; Liu, Y.Q.; Du, T.; Zhang, Z.B. (2009): A new solid-shell element(MSSS) for sheet forming simulation. *Journal of Plasticity Engineering*. In Press.

Zhao, J.J; Hu, Z.H. (2000): Three-Dimension nonlinear finite element analysis of skew rolling of tubular part. *Journal of Plasticity Engineering*, 7(2): 20-23.

